Measuring Total Electron Content with GNSS: Investigation of two different techniques

Conference Paper · May 2009

DOI: 10.1049/cp.2009.0063 · Source: IEEE Xplore

2 authors:

Benoît Bidaine
CE+T Energrid, Liège, Belgium
43 PUBLICATIONS **148** CITATIONS
SEE PROFILE

René Warnant
University of Liège
137 PUBLICATIONS **1,565** CITATIONS
SEE PROFILE

MEASURING TOTAL ELECTRON CONTENT WITH GNSS: INVESTIGATION OF TWO DIFFERENT TECHNIQUES[1]

B. Bidaine*, R. Warnant†

*F.R.S.-FNRS / University of Liège (ULg) - Geomatics Unit
Allée du 6-Août, 17
B-4000 Liège (Belgium)
Email: B.Bidaine@ulg.ac.be

†Royal Meteorological Institute of Belgium (RMI)
Avenue Circulaire, 3
B-1180 Brussels (Begium)
Email: R.Warnant@oma.be

Keywords: Total Electron Content (TEC), Global Navigation Satellite Systems (GNSS), TEC comparison, sTEC calibration, Global Ionospheric Maps (GIMs)

Abstract

The ionosphere widely affects Global Navigation Satellite Systems (GNSS) applications, inducing among others a delay in GNSS measurements. This delay is closely linked to the Total Electron Content (TEC) of the ionosphere, a major parameter which can hence be monitored using GNSS. To this extent, phase measurements are taken as a basis for their lower noise level. Levelling strategies have then to be defined for the phase measurements are obtained with an initial unknown number of cycles called ambiguity.

The most common technique, referred to as carrier-to-code levelling, consists in using the differences between code and phase measurements and their average on a continuous set of epochs. This option, chosen at the Royal Meteorological Institute (RMI) of Belgium to compute TEC for Belgian GPS stations, requires code hardware delays estimation. Another has been proposed which takes benefit from Global Ionospheric Maps (GIMs) to compute a reference TEC used for ambiguity resolution.

In order to understand the consequences of using one method or the other, we compare slant TEC data obtained from both techniques for a mid-latitude station (Brussels) during a high solar activity period (2002). We observed large differences (6.8 $TECu$ on average) showing features apparently related to ionospheric and geomagnetic activity. We attribute these observations to a combination of effects originating in code delays estimation, multipath and noise as well as GIMs errors. We try to differentiate between these effects by focusing on several days and satellites. We concentrate for example on days presenting large TEC differences and geomagnetic disturbances simultaneously (or not) or on satellites displaying recurrent patterns on consecutive days.

Finally we highlight the impact of the choice of GIMs involved in sTEC calibration. To this extent, we analyse vertical TEC statistics showing a general underestimation from RMI data. The highest bias (5.8 $TECu$) is obtained for the UPC GIMs used in the second levelling technique.

1 Introduction

The ionosphere widely affects Global Navigation Satellite Systems (GNSS) applications. Indeed its concentration in free electrons, commonly integrated on satellite-to-receiver paths to obtain slant Total Electron Content (slant TEC or sTEC, in $[electrons\ m^{-2}]$ or more generally TEC units $[TECu = 10^{16}\ el.m^{-2}]$), induces among others a delay in code and phase measurements. The latter depends on the signal frequency (cf. equation 3) and can reach values exceeding 100 m in extreme cases[2].

Consequently monitoring TEC is of prime interest and not only for GNSS applications. It is vitally important for single frequency mode of operation for which sTEC must be modelled in order to provide an adequate correction to the users. To this extent, the US Global Positioning System (GPS) uses the Klobuchar model [5] and the future European Galileo system will rely on an algorithm implementing the NeQuick model [6]. TEC measurements are routinely involved in the update of the information broadcast to the users in the framework of these algorithms. More primarily, they enable the assessment of the performances of these corrections (eg [8]) or the validation and possible improvement of these models (eg [2]).

Scientists have developed different kind of TEC products. Taking benefit from networks of GPS receivers, vertical TEC (vTEC) maps can be computed on a global scale based on the International GNSS Service (IGS) network [4] (Global Ionospheric Maps - GIMs - available from the IGS). Other methods, two of which constitute the scope of this paper, provide sTEC as pri-

[1] Find material about this paper on http://orbi.ulg.ac.be/handle/2268/1553.

[2] A common order of magnitude the $TECu$ is the $16-cm$ error induced for the L_1 carrier (1575.42 MHz).

mary output.

To obtain sTEC, phase measurements are usually taken as a basis for their lower noise level. As they are determined with an initial unknown number of cycles called ambiguity, corresponding resolution - or levelling - strategies have to be defined leading to appreciable differences in TEC evaluation. Levelling can be performed (cf. subsection 2.1) by means

- of code measurements as at the Royal Meteorological Institute (RMI) of Belgium [12] - this case will be referred to as RMI from now on;
- of reference global TEC [9] provided, for instance, by GIMs - this case will be referred to as GIMl from now on.

In both cases, the average of the difference with phase measurements is computed on a continuous set of epochs, called arc, ie a period characterized by the same ambiguity, and provides the unknown.

The comparison of data obtained from both techniques shows differences (constant for continuous arcs as expected from developments in subsection 2.1) which can be attributed

- to receiver and satellite code delays estimation, code multipath or code noise implied by the first levelling technique [3]
- or to the reference TEC associated to the second technique.

To get some insight into the second explanation, we perform a vTEC comparison between RMI data and different GIMs in section 3.

2 sTEC comparison

2.1 Computation process

Code-pseudorange and carrier-phase measurements between receiver p and satellite i for carrier k ($k = 1,2$; frequencies $f_1 = 1575.42\ MHz$ and $f_2 = 1227.6\ MHz$ for GPS) can be formalized by the following equations ($\Psi^i_{p,k}$ for pseudorange and $\Phi^i_{p,k}$ for phase converted to distance multiplying by the wavelength λ_k).

$$\Psi^i_{p,k} = D^i_p + c\left(\Delta t^i(t_e) - \Delta t_p(t)\right) + T^i_p + I^i_{p,k} + M^i_{p,k,g} - g^i_k + g_{p,k} + \varepsilon^i_{p,k,g} \quad (1)$$

$$\Phi^i_{p,k} = D^i_p + c\left(\Delta t^i(t_e) - \Delta t_p(t)\right) + \lambda_k N^i_{p,k} + T^i_p - I^i_{p,k} + M^i_{p,k,\varphi} - p^i_k + p_{p,k} + \varepsilon^i_{p,k,\varphi} \quad (2)$$

D^i_p denotes the geometric distance between satellite i and receiver p.

c denotes the speed of light in free space.

$\Delta t^i(t_e)$ denotes the satellite clock error at time of emission t_e.

$\Delta t_p(t)$ denotes the receiver clock error at time of reception t.

T^i_p denotes the tropospheric or neutrospheric effect.

$I^i_{p,k}$ denotes the ionospheric effect.

$M^i_{p,k,g}$ and $M^i_{p,k,\varphi}$ denote group (g) and phases (φ) multipath effects.

g^i_k, $g_{p,k}$, p^i_k and $p_{p,k}$ denote the biases associated to delays produced by the receiver and the satellite hardware.

$\varepsilon^i_{p,k,g}$ and $\varepsilon^i_{p,k,\varphi}$ denote measurement noises.

N^i_p denotes the integer phase ambiguity, constant for each continuous arc.

Given the ionospheric group delay

$$I^i_{p,k} = \frac{40.3}{f_k^2} sTEC^i_p, \quad (3)$$

it is possible to isolate the $sTEC$ using the geometric free (GF or ionospheric) combinations as follows, neglecting phase multipath and noise.

$$\begin{aligned}\Psi^i_{p,GF} &= \Psi^i_{p,2} - \Psi^i_{p,1} \\ &= I^i_{p,2} - I^i_{p,1} + M^i_{p,2,g} - M^i_{p,1,g} - g^i_2 + g_{p,2} \\ &\quad - (-g^i_1 + g_{p,1}) + \varepsilon^i_{p,2,g} - \varepsilon^i_{p,1,g} \\ &= A\, sTEC^i_p + M^i_{p,GF,g} + g^i_{p,GF} + \varepsilon^i_{p,GF,g}\end{aligned} \quad (4)$$

$$\begin{aligned}\Phi^i_{p,GF} &= \Phi^i_{p,1} - \Phi^i_{p,2} \\ &= -I^i_{p,1} + I^i_{p,2} + M^i_{p,1,\varphi} - M^i_{p,2,\varphi} - p^i_1 + p_{p,1} \\ &\quad - (-p^i_2 + p_{p,2}) + \lambda_1 N^i_{p,1} - \lambda_2 N^i_{p,2} + \varepsilon^i_{p,1,\varphi} - \varepsilon^i_{p,2,\varphi} \\ &= A\, sTEC^i_p + p^i_{p,GF} + N^i_{p,GF}\end{aligned} \quad (5)$$

$$A = 40.3\left(\frac{1}{f_2^2} - \frac{1}{f_1^2}\right) \quad (6)$$

$$*^i_{p,GF,g} = *^i_{p,2,g} - *^i_{p,1,g} \quad (7)$$

$$g^i_{p,GF} = -g^i_2 + g_{p,2} - (-g^i_1 + g_{p,1}) \quad (8)$$

$$p^i_{p,GF} = -p^i_1 + p_{p,1} - (-p^i_2 + p_{p,2}) \quad (9)$$

$$N^i_{p,GF} = \lambda_1 N^i_{p,1} - \lambda_2 N^i_{p,2} \quad (10)$$

To obtain $sTEC^i_p$, we prefer using the GF phase observation Φ_{GF} which is considered not affected by multipath and noise. (As we will only consider one receiver p and one satellite i and every term of the following equations is affected by the same indices, we can omit these indices from now on.) For both levelling techniques, we also neglect phase delays p_{GF} or we consider them constant on one continuous arc. This allows us to incorporate

them in the ambiguity N_{GF} the determination of which we will now focus on.

For RMI levelling, we subtract the GF code combination from the phase combination and we average on each continuous arc. The largest resulting biases come from the group delays. Assuming them constant with time, we can determine them using a long time series (period T) of the GF code combination and modelling the ionosphere by means of a polynomial in latitude and local time. We can neglect code multipath and noise on a long period but not on a single arc. To keep track of these assumptions and residual effects, let's keep residual terms for multipath ($M_{GF,g}$), group delays (Δg_{GF}) and noise ($\varepsilon_{GF,g}$) in the equations.

$$\langle \Psi_{GF} - A\, sTEC_{pol} \rangle_T = \langle g_{GF} \rangle_T \tag{11}$$

$$\begin{aligned} \Psi_{GF} - \langle \Psi_{GF} - A\, sTEC_{pol} \rangle_T & \\ = A\, sTEC + M_{GF,g} - (\langle g_{GF} \rangle_T - g_{GF}) + \varepsilon_{GF,g} & \\ = A\, sTEC + M_{GF,g} - \Delta g_{GF} + \varepsilon_{GF,g} & \end{aligned} \tag{12}$$

$$\begin{aligned} \langle \Phi_{GF} - \Psi_{GF} + \langle \Psi_{GF} - A\, sTEC_{pol} \rangle_T \rangle_{arc} & \\ = N_{GF} - \langle M_{GF,g} \rangle_{arc} + \langle \Delta g_{GF} \rangle_{arc} - \langle \varepsilon_{GF,g} \rangle_{arc} & \end{aligned} \tag{13}$$

$$\begin{aligned} sTEC_{RMI} = \frac{1}{A} (\Phi_{GF} - \langle \Phi_{GF} - \Psi_{GF} + \langle \Psi_{GF} i & \\ - A\, sTEC_{pol} \rangle_T \rangle_{arc}) & \\ = sTEC + \langle M_{GF,g} \rangle_{arc} - \langle \Delta g_{GF} \rangle_{arc} + \langle \varepsilon_{GF,g} \rangle_{arc} & \end{aligned} \tag{14}$$

For GIMl levelling, we use GIMs and the thin shell approximation to compute a reference $sTEC_{GIM}$ (cf. equation 15). The ionosphere is approximated by a spherical layer of infinitesimal thickness at altitude h_i. The $sTEC$ associated to the satellite line-of-sight is then obtained multiplying the $vTEC$ at the piercing point of the ray in the layer, the ionospheric point (IP), by a mapping function. The latter involves the satellite zenith angle at IP χ_{IP}, on Earth surface χ and the Earth radius R_E.

$$sTEC_{GIM} = \frac{vTEC_{GIM}}{\cos \chi_{IP}} = vTEC \left(\sqrt{1 - \left(\frac{R_E \sin \chi}{R_E + h_i} \right)^2} \right)^{-1} \tag{15}$$

Subtracting $sTEC_{GIM}$ from the phase combination and averaging on each continuous arc provide us with a value for the ambiguity which is however affected by residual errors $\Delta sTEC_{GIM}$ including the GIMs and the mapping function errors. Consequently these will remain in the resulting $sTEC_{GIMl}$ as constant values for each continuous arc.

$$\begin{aligned} \langle \Phi_{GF} - A\, sTEC_{GIM} \rangle_{arc} &= N_{GF} - A \langle sTEC_{GIM} - sTEC \rangle_{arc} \\ &= N_{GF} - A \langle \Delta sTEC_{GIM} \rangle_{arc} \end{aligned} \tag{16}$$

$$sTEC_{GIMl} = \frac{1}{A} (\Phi_{GF} - \langle \Phi_{GF} - A\, sTEC_{GIM} \rangle_{arc}) \tag{17}$$

$$= sTEC + \langle \Delta sTEC_{GIM} \rangle_{arc} \tag{18}$$

To compare data obtained from both techniques, we compute $sTEC$ differences which we expect to be constant for continuous arcs considering previous developments.

$$\begin{aligned} \Delta sTEC_{GIMl-RMI} &= sTEC_{GIMl} - sTEC_{RMI} \\ &= \langle \Delta sTEC_{GIM} \rangle_{arc} - \langle M_{GF,g} \rangle_{arc} + \langle \Delta g_{GF} \rangle_{arc} - \langle \varepsilon_{GF,g} \rangle_{arc} \end{aligned} \tag{19}$$

As can be seen from figure 1, we indeed observe very close $sTEC$ differences for successive epochs of each arc. 99% of the sTEC difference standard deviations computed on individual arcs equal less than 0.02 $TECu$. Therefore summarizing the sTEC differences to their average value by arc is relevant.

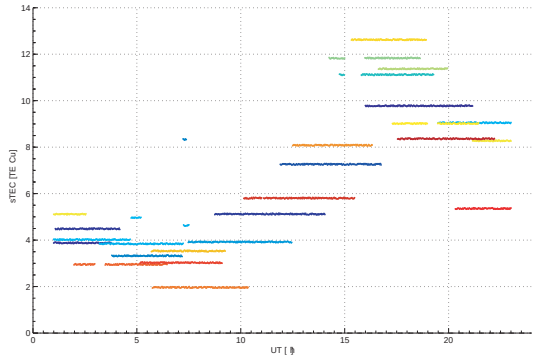

Figure 1: Example of sTEC differences for Brussels station on January 1st, 2002

2.2 Global statistics

In order to compare GIMl and RMI sTEC, we consider the distribution of the average value of the sTEC difference computed on individual arcs. We perform this comparison producing arc sTEC differences using GIMs from Universitat Politècnica de Catalunya (UPC) with the corresponding thin shell height of 450 km, for Brussels station (mid-latitudes: 50.8°N, 4.4°E) over the year 2002 (high solar activity ; cf. figure 2). The global bias and standard deviation (cf. equations 20 and 21) for these 12104 arcs equal respectively 6.8 $TECu$ and 3.5 $TECu$.

$$\text{Bias} = \langle \langle sTEC_{GIMl} - sTEC_{RMI} \rangle_{arc} \rangle \tag{20}$$

$$\text{Std} = \sqrt{\left\langle (\langle sTEC_{GIMl} - sTEC_{RMI} \rangle_{arc} - Bias)^2 \right\rangle} \tag{21}$$

The comparison of the distribution of these arc sTEC differences with the daily average RMI vTEC (cf. figure 3)[3] and the Dst index distributions indicates us a certain degree of ionospheric and geomagnetic activity correlation respectively (correlation coefficient of 0.34 between daily vTEC and daily average of arc sTEC differences). In particular several extreme values of arc sTEC

[3] cf. subsection 3.1 for details about RMI vTEC computation

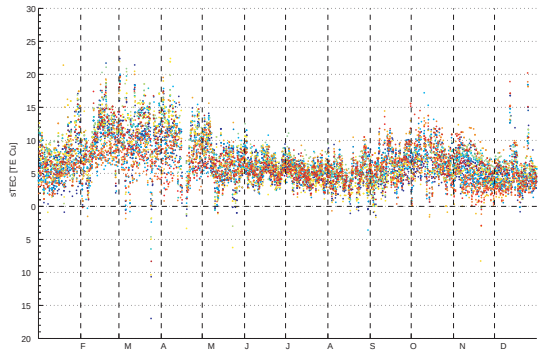

Figure 2: sTEC differences averaged by arc for Brussels station over the year 2002

differences correspond to geomagnetic storms[4] eg around March 24^{th}, April 19^{th}, August 3^{rd} or October 14^{th}.

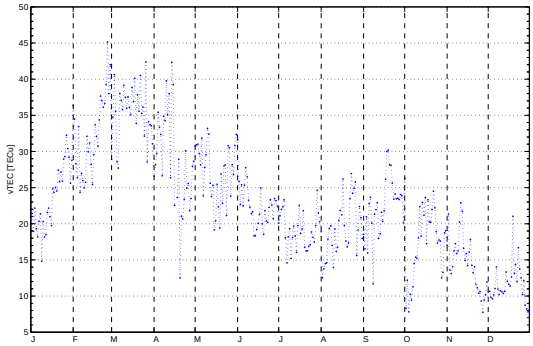

Figure 3: Daily average of RMI vTEC for Brussels station over the year 2002

In order to illustrate the effects behind the arc sTEC differences and possible examples of the biases described in previous section, we choose three days as case studies to investigate more into detail:

- March 24^{th}, 2002 (spring equinox and high ionospheric activity) shows large (negative) differences coinciding with geomagnetic disturbances;
- on December 12^{th}, 2002 (near winter equinox and medium ionospheric activity), we observe large (positive) differences but during a geomagnetically quiet period;
- we finally select August 12^{th}, 2002 as a day with low variability (smallest daily standard deviation) and, hence, average differences (summer and low ionospheric variability, geomagnetically quiet).

[4] To define such storms, one criterium can be chosen as periods with Dst below -50 nT.

2.3 March 24^{th}, 2002

The effect of the geomagnetic storm on March 24^{th} is clearly visible on Dst with a minimum value of -100 nT at 9 UT and vTEC with 76.4 $TECu$ at 12:15 UT.

The large negative sTEC differences visible on March 24^{th} indicate that GIMl sTEC becomes far lower than RMI sTEC contrary to the global trend. In such cases, GIMl sTEC seems to react less to geomagnetic storms than RMI sTEC. The worst situation appears for PRN 2 with a minimum arc sTEC difference of -17 $TECu$ (cf. figure 4). This satellite is visible around midday and has a maximum elevation of 56° which suggests that a certain dependence towards time-of-day and elevation should be investigated. It is clear for instance that elevation has an influence on GIMs residual errors through the use of the mapping function for computing reference sTEC from GIMs vTEC or on code multipath effect.

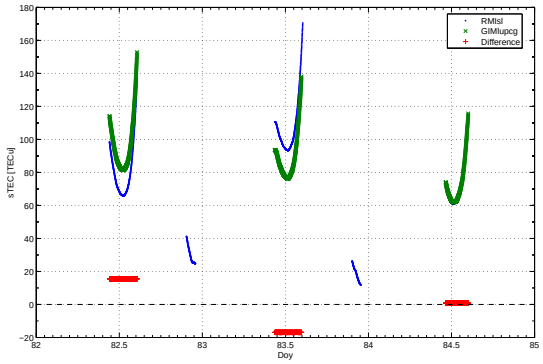

Figure 4: sTEC data and differences for Brussels station between March 23^{rd} to 25^{th}, 2002 for PRN 2

2.4 December 12^{th}, 2002

On December 12^{th}, the second case day, no irregular effect appears in Dst or RMI vTEC but well sTEC differences. GIMs residual errors could then constitute the main origin of sTEC differences.

Focusing on particular satellites, we state a good correlation between arc sTEC differences for PRN 26 and 29 (cf. figure 5). This situation begins on June 27^{th} when a ΔV maneuver stabilized PRN 29 orbit leading to close traces with PRN 26. Such combinations suggest a low influence of satellite delays by comparison to effects related to geometry acting similarly on close satellites and could anyway allow to distinguish between these effects.

2.5 August 12^{th}, 2002

Some correlation with ionospheric activity still exists for this last case day (August 12^{th}) as the arc sTEC differences are lower on this day than on the day before, similarly to vTEC. However the daily range of these values is far lower than in previous case studies with 3.1 $TECu$ for this case versus 28.9 $TECu$ and

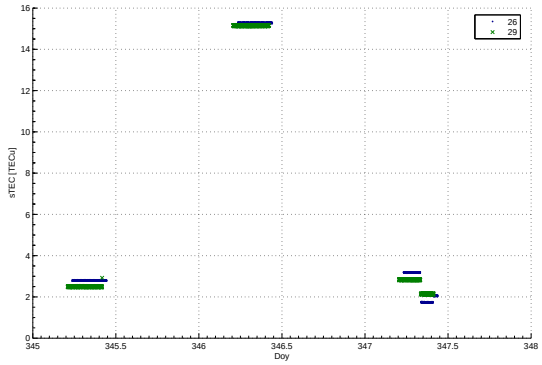

Figure 5: sTEC differences for Brussels station between December 11^{th} to 13^{th}, 2002 for PRN 26 and 29

15.77 *TECu* respectively for the two previous ones.

Comparing the situation for specific PRN between successive days, we note recurrent differences between successive arcs of the same discontinuous visibility period of one satellite. For PRN 15 or 17 for example (cf. figure 6), the visibility period has been divided into two arcs most probably due to cycle slip. Hence two different ambiguities must have been computed and the averaged effects related to RMI levelling described in subsection 2.1 apparently took different values. Indeed we observe a discontinuity for RMI sTEC which remains parallel to GIMl sTEC for the second arc but with a larger difference. The latter could come from a different averaged multipath effect as the second arc is composed of a smaller number of points at lower elevations.

The investigation of these discontinuities appears really interesting as they are quite large and numerous (771 differences larger than 1 *TECu* in absolute value implying 1489 arcs).

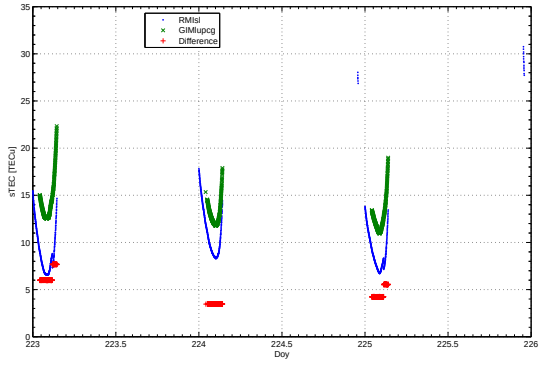

Figure 6: sTEC data and differences for Brussels station between August 11^{th} and 13^{th}, 2002 for PRN 17

3 vTEC comparison

3.1 Computation process

At the RMI, different procedures are applied to obtain *vTEC* representative of the ionosphere above the observing station [12]. All of them begin with a selection of *sTEC* values, converted to vertical using a mapping function associated to a 400-km thin shell height (cf. equation 15) and averaged over 15-minute periods. The method chosen for this study uses the *sTEC* values associated to IP not further that 200 km in latitude or longitude from the station[5].

In the following, these data are compared to *vTEC* computed from GIMs from the different IGS Associate Analysis Centres (IAACs)[6] and to their combination (referred to as IGS). Taking into account their time (2 hours) and space (2.5°in latitude, 5°in longitude) resolutions, linear time interpolation between consecutive rotated maps and bi-linear space interpolation are applied [10].

3.2 Results

A *vTEC* comparison in the same framework than for *sTEC* (cf. subsection 2.2: Brussels station, year 2002) allows us to observe the influence of the choice of reference TEC involved in the GIMl levelling process. Hence we compute the bias and standard deviation of the GIMs sampled with a 15-minute rate regarding the RMI data (cf. table 1).

	Bias [TECu]	Std [TECu]
CODE	2.7	2.0
EMR	5.6	2.9
ESA	0.0	5.6
JPL	5.5	2.1
UPC	5.8	3.2
IGS	4.2	2.1

Table 1: Comparison between RMI and GIMs vTEC for Brussels station over the year 2002

Keeping in mind an order of magnitude for *vTEC* of 23 *TECu* (the yearly average *vTEC* for RMI data), we state a general TEC underestimation for the RMI case by comparison to GIMs. The statistics for UPC GIMs are consistent with the *sTEC* comparison. The use of CODE GIMs would apparently provide the best agreement.

However comparisons of GIMs with TOPEX data tend to attribute the best performances to JPL and UPC GIMs [7]. On the one hand, as classifying the centres according to their performances (eg according to the bias) produces approximately the same order in both studies, we could conclude to a TEC underestimation from the RMI technique. On the other hand, recent

[5] A 200-km circle around the station would correspond to an elevation threshold of 61.8°.

[6] (CODE) University of Bern, Energy, Mines and Resources (EMR, NRCan), European Space Agency (ESA), Jet Propulsion Laboratory (JPL) and Universitat Politècnica de Catalunya (UPC)

results highlight the existence of systematic biases in TOPEX data [1] so that some of the GIMs could actually overestimate TEC.

4 Conclusion

We compared sTEC data computed on the basis of GPS measurements by means of two different levelling techniques, one using code measurements and the other Global Ionospheric Maps (GIMs). For a mid-latitude station (Brussels) during a year of high solar activity (2002), we observed large differences constant by arc between them equalling 6.8 *TECu* on average. We highlighted four possible origins for these biases – code delays estimation, multipath and noise as well as GIMs errors – and stated several correlations with other geophysical parameters and between several situations.

We focused on several case days trying to identify situations characterized by different levels of influence of our four hypotheses. For example we showed large differences (up to 17 *TECu*) concomitant or not with geomagnetic disturbances. We examined day-to-day variability or recurrence, accounting for GIMs or multipath main influence.

We finally investigated the choice of GIMs computing *vTEC* statistics by comparison with RMI data. We observed a general TEC underestimation from the latter dataset, reaching the highest value (5.8 *TECu*) for the UPC GIM selected for *sTEC* calibration. However the latter could in fact overestimate TEC.

Further investigations could advantageously involve arc-to-arc (cf. subsection 2.5), inter-satellite and inter-station comparisons[7] allowing for example to study lower receiver or satellite delays effects. Furthermore the development of triple frequency systems reveals itself very promising as they will enable comparisons with new TEC monitoring techniques [11].

Acknowledgements

The work presented in this paper is part of B. Bidaine's PhD Thesis in progress under a F.R.S.-FNRS fellowship (Belgian National Fund for Scientific Research). Benoît would like to acknowledge Roberto Prieto-Cerdeira and Raul Orus from ESA/ESTEC for providing sTEC data levelled using UPC GIMs and comments about them. The GIMs computed by IAACs were obtained from the International GNSS Service (IGS).

References

[1] F. AZPILICUETA, C. BRUNINI. "Analysis of the bias between TOPEX and GPS vTEC determinations", *J. Geod.*, **81**, 2, (2008). doi:10.1007/s00190-008-0244-7

[2] B. BIDAINE, R. WARNANT. "Towards an Improved Single-Frequency Ionospheric Correction: Focus on Mid-Latitudes", *Proc. 4th ESA Workshop on Satellite Navigation User Equipment Technologies NAVITEC 2008* [CD-Rom], ESA/ESTEC, Noordwijk (The Netherlands), (2008). http://orbi.ulg.ac.be/handle/2268/1551

[3] L. CIRAOLO, F. AZPILICUETA, C. BRUNINI, A. MEZA, S. M. RADICELLA. "Calibration errors on experimental slant total electron content (TEC) determined with GPS", *J. Geod.*, **81**, 2, pp. 111-120, (2007). doi:10.1007-s00190-006-0093-1

[4] J. M. DOW, R. E. NEILAN, G. GENDT. "The International GPS Service (IGS): Celebrating the 10th Anniversary and Looking to the Next Decade", *Adv. Space Res.*, **36**, 3, pp. 320-326, (2005). doi:10.1016/j.asr.2005.05.125

[5] J. A. KLOBUCHAR. "Ionospheric Time-Delay Algorithm for Single-Frequency GPS Users", *IEEE Transactions on Aerospace and Electronic Systems*, **AES-23**, 3, pp. 325-331, (1987). doi:10.1109/TAES.1987.310829

[6] B. NAVA, P. COÏSSON, S. M. RADICELLA. "A new version of the NeQuick ionosphere electron density model", *J. Atmos. and Sol.-Terr. Phys.*, **70**, 15, pp. 1856-1862, (2008). doi:10.1016/j.jastp.2008.01.015

[7] R. ORUS, M. HERNANDEZ-PAJARES, J. M. JUAN, J. SANZ, M. GARCIA-FERNANDEZ. "Performance of different TEC models to provide GPS Ionospheric corrections", *J. Atmos. and Sol.-Terr. Phys.*, **64**, 18, pp. 2055-2062, (2002). doi:10.1016/S1364-6826(02)00224-9

[8] R. ORUS, B. ARBESSER-RASTBURG, R. PRIETO CERDEIRA, M. HERNANDEZ-PAJARES, J. M. JUAN, J. SANZ. "Performance of Different Ionospheric Models for Single Frequency Navigation Receivers", *Proc. Beacon Satellite Symposium 2007*, Boston College, Boston (USA), (2007).

[9] R. ORUS, LJ. R. CANDER, M. HERNANDEZ-PAJARES. "Testing regional vTEC maps over Europe during the 17-21 January 2005 sudden space weather event", *Radio Sci.*, **42**, RS3004, (2007). doi:10.1029/2006RS003515

[10] S. SCHAER, W. GURTNER, J. FELTENS. "IONEX: The IONosphere Map EXchange Format Version 1", *Proc. IGS Analysis Centers Workshop*, ESA/ESOC, Darmstadt (Germany), pp. 233-247, (1998). ftp://igscb.jpl.nasa.gov/igscb/data/format/ionex1.ps

[11] J. SPITS, R. WARNANT. "Total electron content monitoring using triple frequency GNSS data: A three-step approach", *J. Atmos. and Sol.-Terr. Phys.*, **70**, 15, pp. 1885-1893, (2008). doi:doi:10.1016/j.jastp.2008.03.007

[12] R. WARNANT, E. POTTIAUX. "The increase of the ionospheric activity as measured by GPS", *Earth Planets Space*, **52**, 11, pp. 1055-1060, (2000). http://www.terrapub.co.jp/journals/EPS/pdf/5211/52111055.pdf

[7] We gathered similar data sets for Dourbes station.